a 10-fold volume excess of buffer (50 mM citrate phosphate buffer), followed by centrifugation at 10,000*g* in an Airfuge. We obtained X-band continuous wave (CW) EPR spectra by using a loop-gap resonator with 2-mW incident power, 100-kHz modulation frequency, and 1-G modulation amplitude.

21. These spectra contain information about the motional freedom of the spin label and how it is affected by local steric restrictions. In the absence of a formal line shape analysis for each spectrum, the parameter ΔHo, representing the width of the central resonance line, has been successfully used as an empiric measure of probe mobility [H. S. Mchaourab *et al.*, *Biochemistry* **35**, 7692 (1996)]. An increase in ΔHo (a positive ΔΔHo) signals a decrease of motional freedom, perhaps from newly formed tertiary or quaternary contacts. Similarly, a decrease in ΔHo (negative ΔΔHo) indicates an increase in the probe's freedom of movement. For a sample containing multiple spin labels, the spectral line shape can also be affected by the extent of trough-space spin-spin dipolar coupling. Such interactions produce spectral broadening in a distance-dependent manner [G. R. Eaton and S. S. Eaton, in *Spin Labeling. Theory and Applications*, L. J. Berliner and J. Reuben, Eds. (Plenum, New York, 1989)]. At room temperature, this occurs proportionally for distances as large as 15 to16 Å and as small as 7 to 8 Å, at which point direct, collisional spin exchange will likely occur. In systems of two spins, these interactions have been used with impressive accuracy to directly estimate interspin distances [M. D. Rabenstein and Y. K. Shin, *Proc. Nat. Acad. Sci. U.S.A.* **92**, 8239 (1995); E. J. Hustedt *et al.*, *Biophys. J.* **72**, 1861 (1997); H. S. Mchaourab et *al.*, *Biochemistry* **36**, 307 (1997); H. J. Steinhoff et *al.*, *Biophys. J.* **73**, 3287 (1997)], but in a system with fourfold symmetry like KcsA dipolar interactions cannot be reliably translated into actual physical distances. Instead, spectral broadening can be used to estimate changes in overall probe proximity in the form of the Ω parameter (*9*). This is operationally defined as $\Omega = \bar{A}^*/\bar{A}^\circ$, where $\bar{A}^*$ is the amplitude of the central resonance line ($M = 0$), normalized to the total number of spins in the sample, of a fully labeled mutant (containing two or more labels), and $\bar{A}^\circ$ is the amplitude of the central resonance line, also normalized to the total number of spins in the sample, of an underlabeled mutant (containing only one label per tetramer). In this report, we have considered a relative Ω parameter by comparing fully labeled channels in two conformational states, closed and open. Note that under these conditions, the magnitude of Ω can be affected by large changes in probe mobility.
22. We obtained power spectra by applying the discrete Fourier transform evaluated for the value $\omega = \hat{\omega}$ that maximizes $P(\omega)$ [J. L. Cornette *et al.*, *J. Mol. Biol.* **195**, 659 (1987); D. Donnelly, J. P. Overington, T. L. Blundell, *Prot. Eng.* **7**, 645 (1994); see (*9*)].
23. In a rigid body movement of an α helix , the overall α periodicity of a given structural property (ΔHo) is normally preserved. Rotations generate a mobility profile that is shifted along the residue axis, whereas tilts and dissociations primarily affect the side of the helix involved in tertiary or quaternary contacts. In either case, the power spectra will show a prominent peak near 100°. If, on the other hand, there are changes in secondary structure, the relative area of the peak near 100° will decrease according to the magnitude of the loss in helical periodicity.
24. This is the resultant vector from the sum of all ΔHo values in polar coordinates calculated from the equation

$$M(\omega) = \left[\sum_{j=1}^{N} V_j \cos(j\omega)\right]^2 + \left[\sum_{j=1}^{N} V_j \operatorname{sen}(j\omega)\right]^2$$

[D. Eisenberg *et al.*, *Proc. Natl. Acad. Sci. U.S.A.* **81**, 140 (1984)]. The angle θ was obtained as the value of the resultant $M(\omega)$ evaluated at $\omega = 100°$, taking an arbitrary residue as a reference point ($\theta = 0$). Δθ was calculated as the angular difference between θ at neutral pH and θ at acidic pH.
25. Abbreviations for amino acid residues are as follows: A, Ala; C, Cys; D, Asp; E, Glu; F, Phe; G, Gly; H, His; I, Ile; K, Lys; L, Leu; M, Met; N, Asn; P, Pro; Q, Gln; R, Arg; S, Ser; T, Thr; V, Val; W, Trp; and Y, Tyr.
26. This is because the module of the individual vectors (either ΔHo or Ω) is affected by nonstructural factors: Ω is nonlinearly dependent with distance and is affected in an unknown way by the presence of the four interacting spin labels; ΔHo values are closely related to the local steric environment at each individual position, which obviously changes upon channel opening. Therefore, the value of the Δθ angle should be taken as a qualitative estimate of the magnitude of the rotation.
27. This response can be represented by a simple kinetic scheme,

$$C_1 \overset{H^+}{\leftrightarrow} C_2 \overset{H^+}{\leftrightarrow} C_3 \overset{H^+}{\leftrightarrow} C_4 \overset{H^+}{\leftrightarrow} O$$

where C_1 represents the channel conformation with all four subunits in the resting state and each kinetic step is associated with the change of a given subunit to the active state, leading to the fully open state O. This scheme was used recently to describe the gating kinetics of glutamate receptor channels [C. Rosenmund *et al.*, *Science* **280**, 1596 (1998)].
28. This case can be represented kinetically as

$$\left\{\begin{array}{l} C_1 \overset{H^+}{\leftrightarrow} C_2 \\ C_1 \overset{H^+}{\leftrightarrow} C_2 \\ C_1 \overset{H^+}{\leftrightarrow} C_2 \\ C_1 \overset{H^+}{\leftrightarrow} C_2 \end{array}\right\} \leftrightarrow O$$

where the $C_1 \leftrightarrow C_2$ transition represents the measured conformational change that leads to a final, concerted transition to the open state. [F. Bezanilla *et al.*, *Biophys. J.* **66**, 1011 (1994); W. N. Zagotta *et al.*, *J. Gen. Physiol.* **103**, 321 (1994)].
29. C. S. Anderson, R. MacKinnon, C. Smith, C. Miller, *J. Gen. Physiol.* **91**, 317 (1988).
30. F. J. Sigworth, *Q. Rev. Biophys.* **27**, 1 (1994).
31. G. Yellen, *ibid.*, in press.
32. M. L. Chapman *et al.*, *Biophys. J.* **72**, 708 (1997); J. Zheng and F. J. Sigworth, *J. Gen. Physiol.* **110**, 101 (1997).
33. A. Nicholls, K. A. Sharp, B. Honig, *Proteins* **11**, 281 (1991).

34. Support by the National Institutes of Health (grants GM54690 and GM57846) is gratefully acknowledged. We are indebted to R. Nakamoto, M. Wiener, and H. Mchaourab and to the members of the Perozo Laboratory (Y.-S. Liu, C. Ptak, and A. Fay) for insightful discussions and to R. Nakamoto, G. Szabo, H. Mchaourab, and D. Cafiso for comments on the manuscript. R. MacKinnon kindly provided the C-terminal His-tagged KcsA construct and C. Ptak participated in some of the radiotracer flux experiments. E.P. is particularly grateful to S. Mochel for support and encouragement. E.P. is a McKnight Scholar.

27 January 1999; accepted 10 May 1999

REPORTS

SHRIMP Uranium-Lead Dating of Diagenetic Xenotime in Siliciclastic Sedimentary Rocks

Neal J. McNaughton, Birger Rasmussen, Ian R. Fletcher

Diagenetic xenotime is common in siliciclastic sedimentary rocks, where it starts to form on detrital zircon shortly after sediment deposition. It is possible to estimate the age of sedimentary rocks by in situ uranium-lead analysis of that xenotime. Two Proterozoic sandstone units from northwestern Australia, previously constrained to the age interval of 1790 to 750 million years ago, have diagenetic xenotime ages of 1704 ± 7 and 1704 ± 14 million years ago. This method has potential for dating sedimentary sequences of all ages but should be especially valuable for refining the Precambrian time scale.

It is difficult to date siliciclastic sedimentary rocks unless they contain fossils for biostratigraphic division or interbedded volcanic rocks suitable for radiometric dating. Direct radiometric dating of sediment deposition is not possible, but dating early diagenetic minerals can provide close constraints. Several such minerals have been investigated and used for dating (*1*), but none have been found to be routinely applicable over a broad time span. The recent identification of xenotime as an early diagenetic precipitate may provide an alternative, because the mineral is common in siliciclastic sedimentary rocks of all ages (Table 1), generally has high U contents, and retains radiogenic Pb. The mineral is a trace constituent in many lithologies, ranging from shales to conglomerates, deposited in fluvial to marine environments (*2*). Most xenotime overgrowths consist of small (typically <3 μm but can be as large as 30 μm) pyramid-shaped crystals attached to the rounded surfaces of detrital zircon grains (Fig. 1). The euhedral shape of many xenotime overgrowths strongly implies that the mineral formed after sediment deposition. Petrographic textures consistently show that xenotime is engulfed by other diagenetic cements and is clearly one of

Centre for Strategic Mineral Deposits, Department of Geology and Geophysics, University of Western Australia, Nedlands, WA 6907, Australia.

the earliest minerals to form (*2*). The xenotime is interpreted to have started forming immediately below the sediment-water interface as phosphate and Y [as well as rare-earth elements (REEs)] are released into sediment pore waters during the reduction of Fe/Mn-oxyhydroxides and the decomposition of organic matter (*2*). Zircon, which is isostructural with xenotime, provided nucleation sites for precipitation. Here, we show that the dating of xenotime formation can provide a minimum age of sedimentation and probably a close approximation of the age of sediment deposition.

An examination of xenotime from a range of rock types indicates that it is an excellent mineral for U-Pb geochronology. Xenotime has low initial amounts of Pb, high U contents [typically ~1000 parts per million (ppm) for diagenetic crystals and >10,000 ppm for some pegmatitic crystals], and an exceptional ability to remain closed to U and Pb mobility with time.

Procedures for in situ isotopic analysis of authigenic xenotime overgrowths ≥5 μm have been developed with a SHRIMP II (sensitive high-resolution ion microprobe) mass spectrometer, based on those routinely used for zircon (*3*). Substrate zircons were also analyzed, and xenotime data were corrected for contamination due to primary beam overlap onto the zircon. Data have been omitted if the proportion of primary beam overlap onto zircon is >10% or if the age correction is >12 million years.

The Kimberley basin in northwestern Australia is one of the many Precambrian basins where age control is scarce. It consists of a thick sequence of Proterozoic sedimentary rocks (Fig. 2), unconformably overlain by Neoproterozoic glacigene sequences, the oldest of which correlates with the 750-Ma (million years ago) Sturtian glaciation (*4*). The age of the Speewah Group and the lower part of the Kimberley Group (Fig. 2) is constrained to >1790 ± 4 Ma, the age of the Hart Dolerite (*5*), which intrudes up to, and may be coeval with, the Carson Volcanics. The Warton Sandstone, which directly overlies the Carson Volcanics, along with the remainder of the Kimberley basin, is constrained only to the interval 1790 to 750 Ma.

The Warton Sandstone and the overlying Pentecost Sandstone are mature quartz arenites and have a diverse range of heavy minerals. Zircon grains are common and many (60%) have xenotime overgrowths. The xenotime crystals vary from minute (<1 μm) irregular crystals to large (~20 μm) pyramidal overgrowths, some of which display compositional zonation (Fig. 1). Locally, xenotime overgrowths are engulfed by syntaxial quartz overgrowths, and these compose up to ~30% of the rock. In the Warton Sandstone, scanning electron microscope (SEM)–cathodoluminescence examination shows numerous detrital quartz grains that apparently float in nonluminescent quartz cement. The texture implies that quartz overgrowths formed before deep burial and compaction.

We made 34 analyses of 19 overgrowths

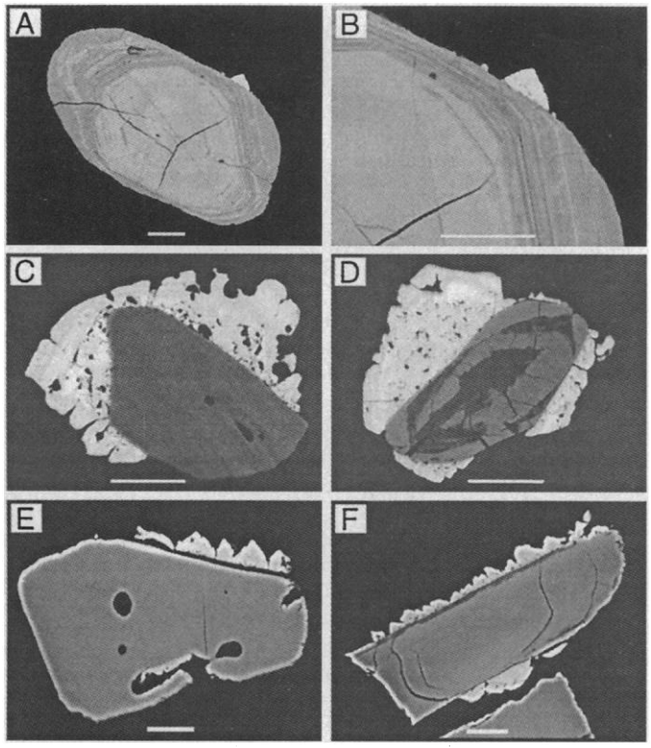

Fig. 1. SEM-backscattered electron images showing detrital zircon grains (light to dark gray) with syntaxial overgrowths of xenotime (white). Scale bars are 20 μm. (**A** and **B**) Rounded detrital zircon grain with a minute pyramidal outgrowth of xenotime (Pentecost Sandstone, Kimberley Group). (**C** and **D**) Rounded zircon grains with large xenotime overgrowths showing compositional zonation and later growth and partial dissolution (Pentecost Sandstone, Kimberley Group). (**E** and **F**) Detrital zircon grains lined by a crust of xenotime crystals (Warton Sandstone, Kimberley Group).

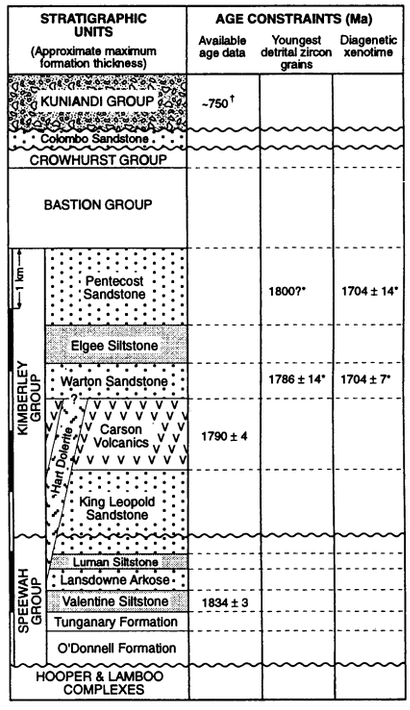

† Glacigene sequences in the Kuniandi Group have been correlated with the 750 Ma Sturtian glaciation

* This study

Fig. 2. The stratigraphic column for the Kimberley basin [after (*7*)], with available published age data [ages for the Valentine Siltstone and Hart Dolerite are from (*5*)].

Table 1. Detrital zircon grain and xenotime overgrowth abundances in siliciclastic sedimentary rocks. Data refer to observations from standard polished thin sections (25 mm by 50 mm) with an SEM.

Age of samples	Number of formations studied	Number of samples studied	Average number of zircons per section	Number of formations with xenotime overgrowths	Number of samples with xenotime overgrowths	Samples with xenotime overgrowths (%)
Phanerozoic						
Mesozoic	4	21	22	3	7	33
Paleozoic	10	110	34	10	54	49
Proterozoic	5	26	36	5	22	85
Archean	6	69	41	5	30	44
Total	25	226	35	23	113	50

(with four analyses rejected for overlap onto zircon) of xenotime for the Warton Sandstone over two analytical sessions. The data [Fig. 3; also see supplementary material (available at www.sciencemag.org/feature/data/1039762)] are not a single age population, but they show a distribution with a strong tail to lower ages. This is interpreted as real age variation due to prolonged xenotime precipitation. Eliminating young ages to produce a symmetric distribution results in a date of 1704 ± 7 Ma (95% confidence limit, n = 24, χ^2 = 0.92). This data subset is still wider than the corresponding Gaussian curve (Fig. 3) and probably still encompasses real age spread in the samples. The earliest xenotime therefore may slightly predate 1704 Ma, but we interpret 1704 ± 7 Ma as an approximate age for deposition of the Warton Sandstone.

Xenotime overgrowths in the Pentecost Sandstone are generally smaller than those in the Warton Sandstone, and they have much lower U contents. In two analytical sessions, almost all data were rejected because of zircon overlap. Subsequently, overgrowths visible under a binocular microscope were carefully oriented for mounting. Most of the useable data (Fig. 3) were from three of those grains. As with the Warton Sandstone, there is a real spread in ages, although it is not as clearly defined because of the smaller number of analyses and poorer precisions, which result from lower U contents. Using the same one-sided data selection as for the Warton Sandstone gives a minimum age of deposition of 1704 ± 14 Ma (95% confidence limit, n = 13, χ^2 = 0.24), with real age spread retained in this reduced data set.

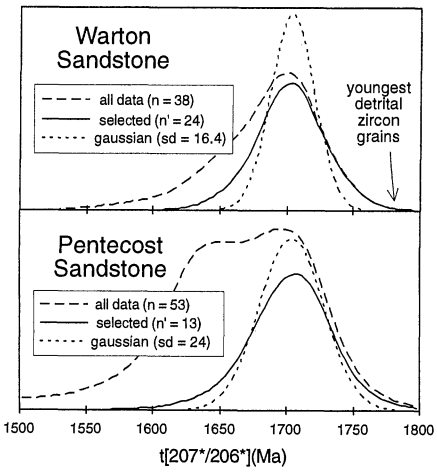

Fig. 3. Probability plots of SHRIMP data for xenotime overgrowths on detrital zircons in the Warton and Pentecost Sandstones. The "selected" data are defined by the removal of younger data points until the remaining profile is symmetric. The Gaussian curve is defined by the standard deviation (sd) calculated from the precisions of the "selected" data points and plotted with the same area as the "selected" curve.

Although xenotimes from the Warton and Pentecost Sandstones cannot be distinguished on the basis of measured age, the chemistry of the xenotime crystals is distinct (for example, 300 to 1100 ppm of U for Pentecost and 1500 to 4000 ppm of U for Warton, with Th/U ratios of 5.0 to 30 for Pentecost and 0.25 to 0.7 for Warton). Clearly, the xenotime crystals from the Warton and Pentecost Sandstones did not precipitate from the same fluid. The crystals were probably derived from chemically distinct pore fluids and commenced forming at different times (but within the errors of the Pb/Pb dates), as the sediments passed through the zone of xenotime precipitation in response to basin subsidence.

SHRIMP data for detrital zircons from the Warton Sandstone (78 analyses on 58 grains) gave ages ranging back to ~2830 Ma (see supplementary material). The youngest 11 grains (27 of 28 analyses) yielded a pooled $^{207}Pb/^{206}Pb$ age of 1786 ± 14 Ma (95% confidence limit, χ^2 = 1.06), within the error of the interpreted age of the underlying Carson Volcanics (>1790 ± 4 Ma). In contrast, of the 35 analyses on 30 grains from the Pentecost Sandstone, only one grain was identified with a possible 1790-Ma provenance; the next youngest had an age of ~1830 Ma (see supplementary material), suggesting substantially different sources for the two units.

The Warton Sandstone is younger than the youngest detrital zircon population at 1781 ± 14 Ma. The approximate age of deposition from diagenetic xenotime is 1704 ± 7 Ma for the Warton Sandstone and 1704 ± 14 Ma for the Pentecost Sandstone. Thus, initial deposition of the sandstones occurred at ~1704 Ma. Therefore, this study also suggests that an appreciable hiatus exists between the Carson Volcanics and the overlying Warton Sandstone.

This study demonstrates that it is possible to date Precambrian diagenetic xenotime crystals as small as 5 μm, achieving a level of precision comparable to U-Pb dating of igneous zircon. Given the ubiquity of diagenetic xenotime, as well as its exceptional properties for U-Pb dating, the geochronology of xenotime may provide ages for siliciclastic sedimentary rocks from Archean to Quaternary terranes [possibly as young as 300,000 years ago (*6*)].

References and Notes

1. Glauconite is the only diagenetic mineral routinely used for dating sediments, and it is most effective for sedimentary sequences of Mesozoic age or younger [P. E. Smith, N. M. Evensen, D. York, G. S. Odin, *Science* **279**, 1517 (1998)]. However, the reliability of isotopic dates derived from this mineral has been questioned [J. D. Obradovich, *Paleoceanography* **3**, 757 (1988)] because it is prone to postdepositional alteration with increasing temperature and pressure. Besides glauconite, clay minerals such as illite have also been used with some success; however, uncertainties about the origin (diagenetic versus detrital) and the timing of closure remain a problem. More recently, authigenic monazite has been dated from Silurian rocks in Wales [J. Evans and J. Zalasiewicz, *Earth Planet. Sci. Lett.* **144**, 421 (1996)], and although promising, the temporal, spatial, and lithological distribution of this mineral is not yet well documented.
2. B. Rasmussen, *Am. J. Sci.* **296**, 601 (1996); _____, R. Buick, W. R. Taylor, *Earth Planet. Sci. Lett.* **164**, 135 (1999).
3. Detrital zircons with xenotime overgrowths are mounted in epoxy disks and sectioned by polishing. An SEM is then used to identify xenotime overgrowths that are sufficiently large for analysis. SHRIMP procedures follow those for zircons [J. B. Smith *et al.*, *Precambrian Res.* **88**, 143 (1998)] except that a retardation lens is used as a precaution against scattered ions from potentially large REE oxide mass peaks that are close to the Pb peaks. An O_2^- primary beam of ~1 nA is focused on a spot with a diameter of ~10 μm. Mass resolution is ≥5000. When reliable U/Pb determinations are essential, the spot should be entirely on xenotime, but for Precambrian samples, for which $^{206}Pb/^{207}Pb$ ages are more precise than $^{206}Pb/^{238}U$ ages, the spot may overlap the surrounding resin. When the sample fills <50% of the primary ion beam spot, Pb/U and U content data can be severely perturbed (see supplementary material). For this reason, much of the xenotime Pb/U data, particularly for the Warton Sandstone, are unreliable, and only Pb/Pb data are reported. The spot can also overlap onto adjacent zircon, and Zr_2O^+ is measured to monitor the degree of overlap. The resulting data corruption (age mixing) can be corrected, in principle, if the age and Pb content of zircon adjacent to the xenotime are independently analyzed. In practice, large corrections are unreliable (see supplementary material). Using $^{207}Pb/^{206}Pb$ dates carries an implied assumption of concordance. During analyses of numerous putative standard xenotimes, the "full-spot" analyses included here, and trial analyses of large (up to 25 μm) ~300-Ma overgrowths, we have seen no evidence for discordance on a scale that would substantially affect the dates reported here. Determination of U/Pb is further hampered by the lack of a xenotime standard with appropriate trace element abundances. Analyses reported here use an interim in-house standard from an Archean pegmatite. This is a multigrain sample, with ~1% U, known from thermal ionization mass spectrometer analyses to be concordant to within ~2%.
4. R. P. Coats and W. V. Preiss, *Precambrian Res.* **13**, 181 (1980).
5. R. W. Page and S.-S. Sun, *Geol. Soc. Aust. Abstr.* **37**, 332 (1994).
6. S. J. A. Brown and I. R. Fletcher, *Geology*, in press.
7. T. J. Griffin and K. Grey, *West. Aust. Geol. Surv. Mem.* **3**, 293 (1990).

8. We thank B. Krapez, R. Buick, R. Ramsay, B. Griffin, I. Tyler, A. Kennedy, J. Evans, and D. Groves for comments and M. Dahl and M. Godfrey for technical expertise. B.R. is supported by an Australian Research Council (ARC) Fellowship. Zircons and xenotimes were analyzed on the SHRIMP II operated by a consortium consisting of Curtin University of Technology, the Geological Survey of Western Australia, and the University of Western Australia, with the support of the ARC.

3 March 1999; accepted 18 May 1999